

Design, Development and Preliminary Assessment of a Force Sensor For Robotized Medical Applications

Nitish Kumar, Olivier Piccin, Laurence Meylheuc, Laurent Barbé, Bernard Bayle

Abstract—This paper presents the design, development and the preliminary assessment of a force sensor designed for robotized medical applications. The requirements and constraints for the force sensor are derived from the targeted application of needle insertion in the context of interventional radiology. These constraints rule out the feasibility of commercially available force sensors necessitating the design of a novel force sensor. A discussion on the various force sensing principles utilized in medical robotics and the choice of a suitable sensible principle is done. Next, the solution principles are offered for the design of the flexural element. Starting from the rigid body equivalent, a compliant model of the flexural element is obtained. Simulation using FEM analysis is utilized to verify that the force sensor indeed satisfies the requirements and the constraints of the targeted application. Finally, the calibration and the experimental validation of the force sensor prototype is done using a realistic force profile showing actual force variation during needle insertion.

Index Terms—Sensors and Sensing Systems, Medical Robotics/Mechatronics

I. INTRODUCTION

With the development of medical robotic assistants and the creation of an interface between the patient and the physician in a teleoperation scenario [1], direct contact with the patient is lessening. One important aspect is the feel of the forces while the practitioner is operating on the patient, for instance the interaction forces with the needle and the tissue. Hence, haptic force feedback has become a necessity to provide physicians with this important piece of information. This tactile feedback can help physicians to detect transitions between organs and different tissue layers while inserting a needle. It can also help him to detect key events during the procedure like rupture of tissues.

Medical interventions are increasingly being performed under imaging modalities like X-ray imaging (CT scanner), MRI. These imaging modalities, despite providing useful visual feedback, impose certain constraints upon the tools and devices which could be used with it. For example, MRI does not allow any ferromagnetic material within its vicinity. With-in the context of this paper, limitations imposed by interventional radiology and the medical interventions carried out under CT-scanner would be considered. Certain materials under the CT-scanner produce artifacts and have a distorting effect on the reconstructed image of the needle.

N. Kumar, O. Piccin, L. Meylheuc, L. Barbé and B. Bayle are with the automatic, vision and robotics team of the ICube laboratory, University of Strasbourg, INSA strasbourg and Image-guided Hybrid Surgery Institute (IHU Strasbourg), France. Email: nitish.kumar@etu.unistra.fr

The availability of adapted force sensors is a limiting factor to provide the desired haptic feedback since most of the commercially available force sensors are metallic or are predominantly made of metallic materials. These materials are neither compatible with the MRI nor with the CT-scanner. Several papers [2], [3] can be found on the development of the force sensors for purpose of force feedback, compatible with MRI. The range of forces as well as the degrees of freedom (DOF) of these force sensors vary depending on the medical intervention. These sensors have either redundant DOF or are not adapted to the specific requirements, as detailed in the next section, arising from the needle insertion interventions under CT scanner. These requirements also include the constraints originating from integration of the force sensor into a robotic assistant. Limited works exist on the design of force sensors compatible with CT-scanner for measuring needle insertion forces during percutaneous interventions.

The main objective of this paper is to focus on the design, development and the experimental assessment of a novel force sensor compatible with the CT-scanner, which can provide the radiologist with the much-needed haptic force feedback during needle insertion procedures. This force sensor is to be mounted between an insertion device and a grasping device [4]. It is shown in a broad teleoperation scenario depicted in Fig. 1, where the radiologist at the master station controls the robotic assistant at slave station.

II. REQUIREMENTS STEMMING FROM THE TARGETED APPLICATION

The needle insertion procedures carried out under CT-scanner with the help of a robotic assistant pose their own set of constraints and limitations. The tunnel of a CT-scanner, which has to accommodate the robotic assistant as well as the patient, does not have a large volume. This constraint on the overall size of the robotic assistant imposes the constraint

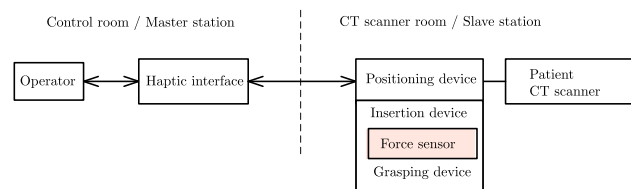


Fig. 1. The force sensor within the general layout of the teleoperated percutaneous procedures.

of size and volume on the force sensor as well. A volume of $25 \times 25 \times 25 \text{ mm}^3$ is imposed on the fabrication of the prototype force sensor in this paper. There could be two approaches for the integration of the force sensor within the robotic assistant. In the first scenario, the axis of the force sensor could have an offset from the axis of the needle and it is far from the point of insertion on the skin. In the second scenario, the axis of the needle crosses the force sensor and the force sensor is as close as possible to the point of insertion on the skin. The second scenario produces a more compact design, as it eliminates any intermediate mechanisms for the transmission of force from the needle to the force sensor. But it also introduces the constraint that the needle must pass through the force sensor. Fulfilling this requires that the force sensor has a hole throughout its body to allow for the passage and the sufficient orientation of the needle.

In its most general context, the purpose of a force sensor is to give the measure of the interaction forces/moments between the needle and the tissues. Since these forces/moments have six components, it would require a 6-DOF sensor for the complete measure. In the work of Maurin *et al.* [5], *in vivo* study of forces during needle insertions was carried out. During this study, it was found that the measure of forces and moments in directions other than the needle axis were approximately 2.10^{-3}N and 6.10^{-3}Nm which are very small compared to the axial force/moment. Hence, the design of a 1-DOF sensor is required which is capable of measuring the needle interaction forces along the needle axis and rejecting the moment disturbance along the same. The above study also revealed that the maximum force of insertion along the needle axis can reach approximately 4N for insertion into the liver including the puncture of the skin. With direct access to the organ, a maximum needle insertion force of 0.7N was recorded, while a minimum resolution of 0.1N was required for detecting the event of capsule puncture. Hence, the nominal rated force for this force sensor has been put to 10N. To provide a security factor, the design study as well as experiments will explore forces up to 25N. For haptic feedback, a very accurate and a very precise sensor is not a requirement. Though it should provide enough resolution and bandwidth for capturing the required haptic information. In the work [6], the frequency analysis of a typical needle insertion force profile shows that the power of insertion forces are concentrated mostly in the frequency range 0 – 2Hz. Hence, a bandwidth up to 2 – 3Hz would be sufficient to measure the interaction forces without significant attenuation. Though no specifications for accuracy and linearity levels are put beforehand, they will be derived from the experimental results. Since the force sensor lies on the axis of the needle, its deformation (less than 0.5 mm) should be very small compared to the insertion length of the needle (25 mm). In other words, the force sensor should have high stiffness along the needle axis. Furthermore, it should have enough rotational stiffness along the needle axis to reject any moment disturbances. The material of the force sensor has to be chosen so as to allow for radiolucency and

compatibility with the CT-scanner.

III. FORCE SENSOR DESIGN

The force sensor design has two aspects : the choice of a sensing principle and the design of the flexural elements.

A. Choice of the Sensing Principle

The development of the force sensors dedicated to medical robotics has been focused on the MRI compatibility [7], [8], which has more stringent requirements than the CT-scanner compatibility. Many of the MRI compatible sensors use optical fibers and sensing principles based on reflection of the light. MRI requires negligible electromagnetic interference (EMI) sensitivity and to this purpose the optic fiber sensors suit the needs of MRI very well. In the work [9], a uniaxial force sensor using optic fibers compatible with ultrasound imaging was developed for minimally invasive surgery. In contrast, CT-scanner does not have such strict requirements of low EMI sensitivity. Hence, sensing modalities based on other principles than reflection of light and optical fibers can be envisaged. An objective of this research work is to design a force sensor that could be cheaper and easier to implement in a whole robotic assistant than sensors based on optic fibers which may be difficult to route on the moving parts. Moreover, optical fiber based force sensors usually require an amplification mechanism as they cannot directly measure very small deformations.

To counter these disadvantages, a sensor design based on strain gages is being taken up. It should be noted that the custom design of the force sensors based on strain gages in the field of medical robotics and for needle insertion procedures is not new. For example in [10], a three DOF force sensor based on strain gages is utilized to measure the interaction forces between the tissue and needle. But as the force sensor is at offset from the needle axis, it cannot directly give the important measure of the axial force. The measurement of the axial force is done indirectly taking into account an intermediate mechanism which is not desirable for the transparency of the measure of the actual needle insertion force. This design does not satisfy the requirement of needle axis coincident with the that of force sensor listed in the section II.

Strain gages have other advantages including ease of construction, simplicity of operation, capability of measuring very small strains without the need for strain amplification mechanisms. Strain gages do not add much to the size and the weight of the force sensor. Due to these advantages, the force sensing based on the strain gages is selected for the construction of the CT-scanner compatible force sensor.

B. Design of the Flexural Element

1) *Choice of architecture:* The classification of flexural elements for force sensing has been extensively studied in the field of force measurement [11]. The flexural elements should enable a small displacement of the force sensor platform along the direction of the needle axis in order to cause the insertion force to develop a work. This displacement

needs to be minimized to keep the flexural elements within their elastic domain of operation as well as to maintain the accuracy of positioning of the distal tip of the needle. The displacements along transverse directions and the rotations along any directions must be as small as possible to reject unwanted contributions of the mechanical actions acting on the needle. The simplest mechanism obeying the aforementioned objectives would have only 1 DOF in translation.

The direct construction of such one translational kinematic function using sliding surfaces, eg. with one or more P joints, is not desirable and would provide incompatible high friction and jamming. A classical constructive approach to limit these drawbacks consists in using linkages with revolute joints in the place of sliders. Within the family of straight-line mechanisms, the Sarrus linkage was found to be an appropriate candidate for the application, since it could allow enough space for the through passage of the needle. This type of mechanism has already been used for other purposes implying large translational motions. For instance, a fully compliant Sarrus mechanism was selected in [12] to design large displacement translational units for mobile robots. Our goal in the present paper will be to use the translational property of the Sarrus mechanism around a given static configuration with only small displacements.

The Sarrus linkage is an overconstrained parallel mechanism with a 2-3R architecture consisting of two legs. Each leg has a set of three parallel adjacent revolute joints. The directions of joints in each leg form a non-zero angle with each other generally fixed at $\frac{\pi}{2}$ as described in Fig. 2(a). The mobility of this mechanism is one DOF in translation and its direction is parallel to the z-axis of the base. To improve the overall rigidity of the assembly, the number of legs can be augmented to three or more. In the present work, the study has been limited to the case of a 4-leg Sarrus mechanism in which two additional 3R legs can be mirrored with a plane of symmetry as shown in Fig. 2(b). As this duplication of legs augments the capacity of this one translational DOF mechanism to better sustain any mechanical actions but the forces along the axis (O_f, z), this 4-3R architecture for the force sensor is retained.

2) *Construction of a compliant mechanism:* The ideal rigid body model of the 4-leg Sarrus mechanism can be

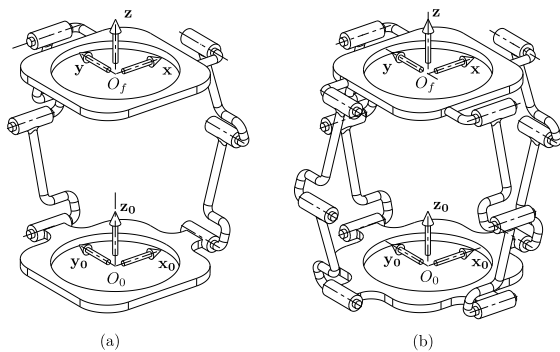


Fig. 2. Sarrus mechanism (a) and its mirrored version with four legs (b).

converted into a corresponding compliant model by replacing some of its revolute joints with equivalent deformable joints. For sensing both tensile and compressive strains, the two links of each 3R chain are replaced by one single flexure element as depicted in Fig. 3. The attachment of each flexure element to the base and the platform is left unchanged with two revolute joints. Thus the resulting compliant Sarrus mechanism (CSM) can be considered as a deformable structure with a certain compliance along the direction z allowing the measurement of the desired axial force. Each flexure member or arm consists of a curved plate with the geometry described in Fig. 4. The width, height and global thickness of the plate are denoted by w, h and e_1 , while its curved shape is given by a circular arc of radius r_1 .

To account for the second revolute joint of the original Sarrus mechanism and favor the localized bending of the flexure members, the central part of each arm has a thinner thickness $e_2 = 0.8e_1$. Given the objective of smaller size required for the force sensor, the design variables h and w are considered as fixed parameters. When submitting the force sensor platform to a force loading along $-z$, the arms bend and the maximum tensile and compressive strains develop on the central thinner part of the outer and inner surfaces S_1 and S_2 of the flexible arms. Hence, the thinner central part of these surfaces will be selected for bonding the strain gages.

3) *Material characterization:* The material of the flexural element has to be radiolucent. The selected material was a DM-8530-Grey60 polypropylene-like digital material used with a Connex 350 rapid prototyping machine. The material characterization pertaining to the Young's modulus and yield strength was carried out on samples using uniaxial tensile loadings in accordance with the ISO 527-1 stan-

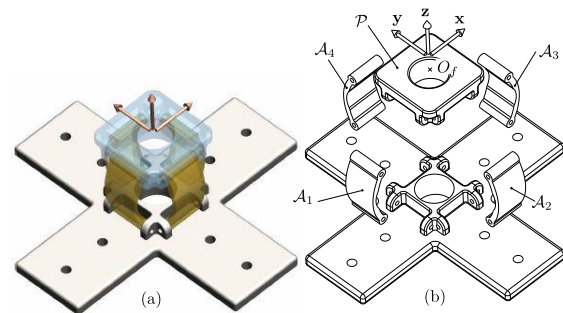


Fig. 3. Compliant Sarrus mechanism CAD view (a) exploded view (b).

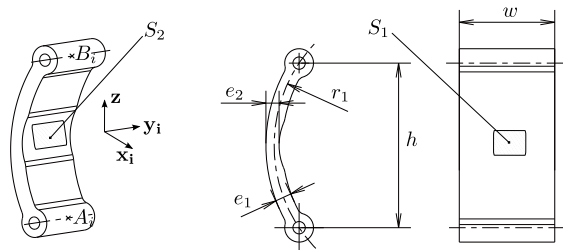


Fig. 4. Geometry of a flexure member.

standard. The test samples were produced in the same material and a similar orientation than the one used for fabricating the flexure elements. The test results have identified a tensile modulus of 750 MPa and a yield strength of 22.5 MPa.

C. Simulation Setup

A simulation setup has been constructed for checking the response of the CSM to various loading cases under different geometric configuration of the flexible arms driven by the structural parameters r_1 and e_1 . Given the geometry of the CSM, the beam or plate theory cannot be used to obtain a closed-form structural model. Based on the CAD model depicted in Fig. 3, a finite element model of the assembly has been prepared. The simulation model includes the four arms \mathcal{A}_i , the platform \mathcal{P} and also describes the axes of the pin joints connecting the arms to the base and the platform.

1) *Boundary and loading conditions:* The simulated actions on the CSM platform are represented by a wrench $\hat{\$}$ composed of a force \mathbf{F} passing through the point O_f and a moment \mathbf{M} . The pin joints located at A_i and B_i on each arm have been modeled using beam elements describing the joint axes for which the rotation freedom about their axis has been released. The stiffness of these beam elements was set to fulfill the rigidity assumption for the axes of the pin joints. Lastly, the rigid modes of the base part have been blocked.

2) *Model setup:* As the CSM is assumed to undergo small displacements around its initial configuration, it can be studied using linear elasticity and the effects of the most general action $\$$ can be obtained by linear superposition of the effects of unit forces and moments projected along the x , y and z axes. As it will be detailed later, stress and strain levels are expected to stay largely under the yield point of the material and thus, the material properties are assumed to be linear and elastic.

D. Results

1) *Study of the axial loading:* The effects of an axial force applied to the CSM platform at point O_f and along $-z$ have been studied.

a) *General behavior of the CSM:* Several simulations have been conducted for different variants of the arms using variable values of the thickness e_1 and the radius r_1 and show that the strains of the CSM are always concentrated in the central part of each arm as depicted in Fig. 5. As expected, the outer and inner surfaces of the arms are respectively submitted to tension and compression. Furthermore, the compressive strain level is always higher by a 1.5 factor than that of the tensile strain whatever the tested parameters e_1 and r_1 . Lastly, the strains remain nearly unchanged along the y_i direction.

b) *Influence of the design parameters e_1 and r_1 :* The Fig. 6 shows both tensile and compressive strains of the arm when the CSM is submitted to an axial force $\mathbf{F}_z = -25\mathbf{z}$ N with the values of the design parameters (e_1, r_1) taken in $\{1.8; 2.0; 2.2\} \times \{14; 16; 18; 25; 28\}$. The variations of e_1 and r_1 affect the resulting stiffness of the

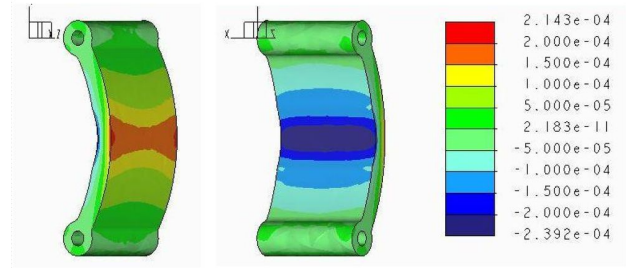


Fig. 5. Strain (ϵ_{zz}) of the flexible arm under unit load along $-z$.

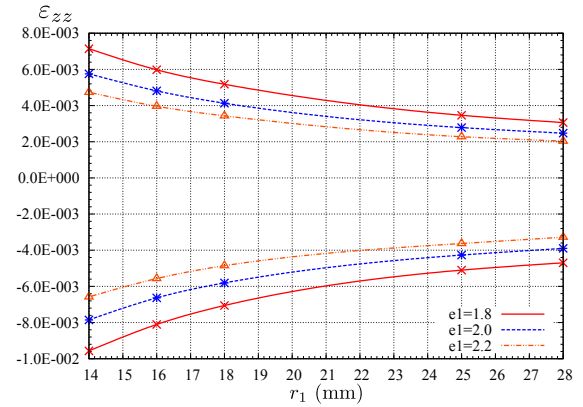


Fig. 6. Variation of the strain (ϵ_{zz}) in function of r_1 and e_1 , for a 25N force applied along $-z$.

CSM in a nonlinear manner despite the assumption of small displacements. Logically, it can be noted that the increase of the arm thickness e_1 raises the stiffness of the CSM and in turn reduces the strain level $|\epsilon_{zz}|$. In the same line, augmenting the radius r_1 also leads to a stiffer CSM since the arms would experience more compression than bending. As bending rigidity is generally lower than compression rigidity, the design parameters should be chosen so as to favor the bending behavior in order to gain a wider range of strain variation. Hence, the radius can be chosen such as $r_1 \leq 18$ mm.

c) *Selection of r_1 and e_1 :* The simulations show that the maximum strains for the worst case ($F = 25\text{N}$, $e_1 = 1.8$, $r_1 = 14$) rise to $|\epsilon_{zz}|_{max} = 10^{-2}$ which is compatible with the $5 \cdot 10^{-2}$ strain limit of most standard strain gages. However, to sustain occasional overloads without a risk of failure, we decided to set the maximum strain to $|\epsilon_{zz}|_{max} = 6 \cdot 10^{-3}$. This restricts the possible parameter sets to $(e_1 = 2.0, r_1 = 18)$, $(e_1 = 2.2, r_1 = 16)$ and $(e_1 = 2.2, r_1 = 18)$. To improve the strain sensitivity at low force loadings, the set $(e_1 = 2.0, r_1 = 18)$ was finally selected since the other two design sets with $e_1 = 2.2$ have lower strains.

2) *CSM stiffness:* The calculated stiffness and the platform displacement along z when submitted to 25N axial force turns out to be 156N/mm and 0.16mm, respectively. This displacement along z is less than 0.5mm. The calculated torsional stiffness and the rotation of the CSM about z when submitted to a 25mN·m moment turns out to be

$6.7 \cdot 10^5 \text{mN}\cdot\text{m}/\text{rad}$ and $3.7 \cdot 10^{-4} \text{rad}$, respectively. Under this load, the maximum strain at the place where the gages will be located is $|\varepsilon_{zz}|_{max} = 1.1 \cdot 10^{-7}$. The platform rotation as well as the corresponding strains in the arms remain negligible, thus this torsional load does not disturb the axial force measurement.

3) *Fabricated prototype*: The parts composing the CSM with $(e_1 = 2.0, r_1 = 18)$ have been produced in rapid prototyping with a Connex 350 machine and assembled using carbon axles. To facilitate the gage setup, dual-pattern gages were chosen and glued onto the outer surface S_1 of the arm \mathcal{A}_1 and the inner surface S_2 of the arm \mathcal{A}_3 to form the four branches of a Wheatstone bridge. Dual-pattern gages were preferred over single element gages owing to less inaccuracies and errors while sticking the gages to the bonding surfaces of the CSM. The dimension of each gage is $7.4 \times 5.8 \text{mm}$.

IV. EXPERIMENTAL ASSESSMENT

In this section, the experimental assessment of the fabricated prototype sensor is carried out. Firstly, the static calibration of the sensor is performed. Then, the results are compared to the ones obtained when a force profile with constant rate of force increase or decrease is applied. Thirdly, the harmonic response of the sensor is analyzed over a reasonable frequency range. Finally, a realistic needle insertion force profile obtained from *in vivo* data is applied to the force sensor. The sensor calibration is discussed based on the three previous calibration experiments and validated on this data set.

A. Experimental Setup

Two experimental setups presented in Fig. 7 were used for the characterization of the prototype force sensor. On the left, the experimental setup consists of a traction machine from Zwick, GmbH (Z005 THN - Allround Line), able to apply varying magnitudes of force and adjustable rates of change of force to the cross-head. The essential components of the experimental setup, namely the cross-head, the calibrated force sensor (XForce HP 50N with an accuracy class 0.5 to ISO 5893 and NF ISO 7500-1) and the prototype CSM force sensor can be seen. The force is applied to the cross-head by the traction machine, which in turn applies the force on top of the prototype force sensor. The traction machine force sensor



Fig. 7. Experimental setups.

is used for the calibration of the prototype through constant force rate input experiments. Though extremely accurate, this setup cannot provide arbitrary force profile as input. Hence, another setup was used for the harmonic response and to provide realistic or experimental force profile as input. This second setup is on the right of Fig. 7. It consists of a two DOF system (X-Y table from Nanomotion) on which a calibrated force sensor (Scaime-K1107-20N) is mounted. In the following, only one DOF is used, so as to apply axial forces to the prototype sensor as input. In both experimental setups, the voltage signal from the Wheatstone bridge of the prototype is fed to a signal conditioner which in turn is acquired by a computer. Since the CSM force sensor is designed to function in the elastic range, a linear relationship between the input and output is expected. The calibration then consists in finding the best correspondence between the input in newtons and the output in volts.

B. Static Experiment

This first experiment corresponds to what is generally called the sensor calibration. Different loads are successively applied to the prototype. Between two different loads, the time delay is far sufficient for the sensor signal to be stable. Each value gives one point of the static characteristics, that is pictured in Fig. 8. A least square fit is applied to obtain the gain and offset required to derive the force value from the electrical measurement. The obtained gain is $0.37 \text{V}/\text{N}$. The linearity error of the force sensor is calculated to be 4.6%. With this fitting, the maximum deviation of the designed sensor output value remained within $\pm 0.5 \text{N}$ with respect to the ideal sensor value. The sensor has lower accuracy when measuring smaller values. Accuracy of the sensor might improve if a non-linear fitting is used to compensate for the non-linearities.

C. Resolution

A resolution of 0.1N was stated in the specification to be achieved by the sensor. To determine its resolution, a rectangular wave signal of 0.1N as shown in the Fig. 9 was applied as an input to the prototype force sensor. In response to each increment, the sensor registers an increment of roughly 0.1N but also reveals an increase in the sensor mean voltage output in function of time. This drift in the

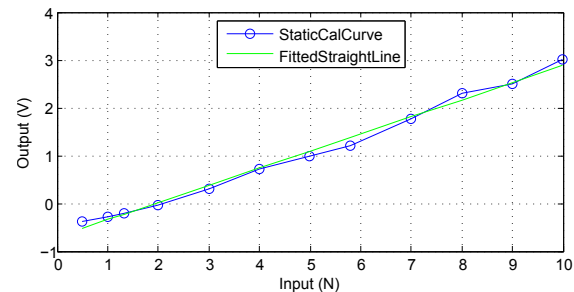


Fig. 8. Static calibration.

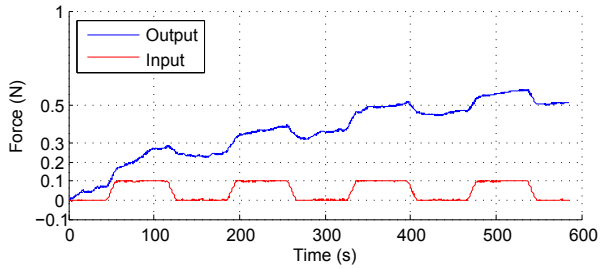


Fig. 9. Test for a resolution of 0.1N.

mean value shows that the inherent non-linearities can not be modeled by a simple gain of 0.37V/N .

D. Constant Force Rate Input Experiment

In this second experiment, a sequence of linear force profiles is applied to the force sensor by the traction machine. The applied force increases linearly up to 25N at a rate of 1N/s . Then it decreases linearly to 0N (slightly more, so as to maintain contact) at -1N/s . The applied force is measured by the traction machine force sensor, while the electrical signal of the prototype force sensor is acquired separately and synchronized. The force and electrical measurement curves are respectively presented in Fig. 10(a) and (b). The rate of increase/decrease of the two measurements are compared. This is performed in the most linear part of the response, so as to characterize the sensor gain value. A total of 32 calibration curves were used which resulted in the 64 slope values. The slopes in the output curves were calculated. A mean slope value of 0.33V/s was calculated corresponding to the rate of change of 1N/s . This gives finally a mean gain value of 0.33V/N . The calibrated curve with this mean gain value is shown in Fig. 10(c).

However, it must be remarked that the obtained results do not correspond to an ideal sensor, i.e. with pure stiffness. The force vs deformation plot in the Fig. 11 is interesting, since it presents an hysteresis that results from a viscoelastic behavior of the sensor. This emphasizes the fact that a purely static model of this sensor is a approximation. It could however be refined by estimating the viscoelasticity of the

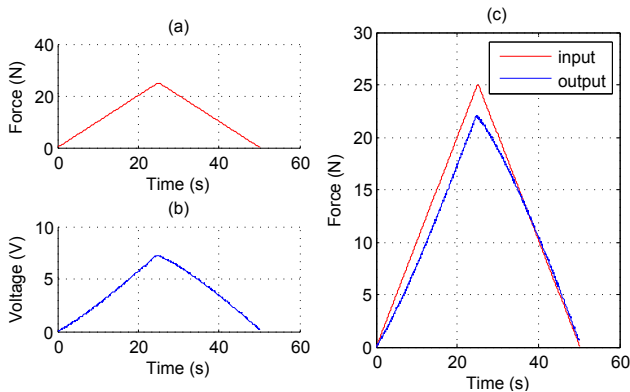


Fig. 10. Calibration curve:(a),output curve:(b),calibrated curve:(c).

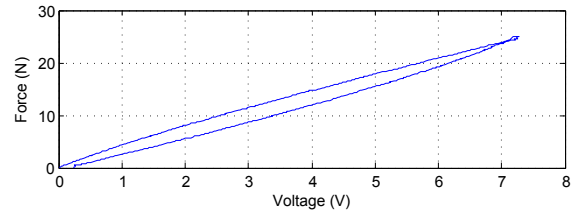


Fig. 11. Force/Voltage plot showing hysteresis

system.

E. Harmonic Response

Then a simple frequency analysis was performed on the prototype sensor over a reasonable frequency range, i.e. between very low frequencies, here 0.01Hz , and the higher frequency compatible with the setup, i.e. 10Hz . At higher frequencies the level of vibrations increased notably and it was preferred to limit the study rather than to have inconsistent results, or even to break the sensor. The Bode magnitude plot, resulting from a set of 14 sinusoidal excitations applied to the prototype sensor, is given in Fig. 12. The measured gain varied from a minimum of 0.19V/N at 4Hz to 0.28V/N at 0.01Hz , which corresponds roughly to a 3 unit change. At 0.5Hz , the value of the gain turns out to be 0.25V/N , which is the middle value over the frequency range. It can be observed that these values are lower than the ones obtained in the static experiment or at constant force rate input experiments (respectively 0.37V/N and 0.33V/N).

This variation is probably due to the influence of the viscoelastic effects, and potentially due to nonlinearities in the prototype structure, resulting from its fabrication process. These effects vary with frequency and the simple elastic modeling associated to the constant gain hypothesis cannot describe the complexity of the sensor prototype. However, it is observed in the next paragraph that this very simple modeling is compatible with the good perception of the haptic information contained in a realistic force signal.

F. Validation

A final validation of the prototype force sensor was done using an input force profile obtained from an actual needle insertion procedure carried out on a pig (Fig. 13). This force profile was earlier presented in [1]. The fit between the

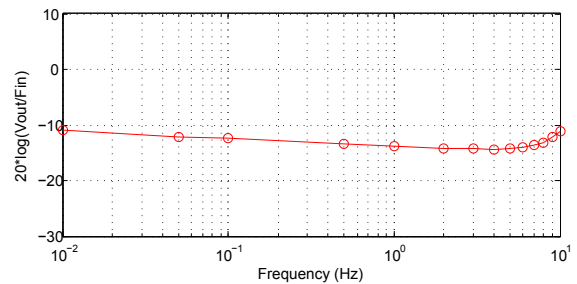


Fig. 12. Bode magnitude plot.

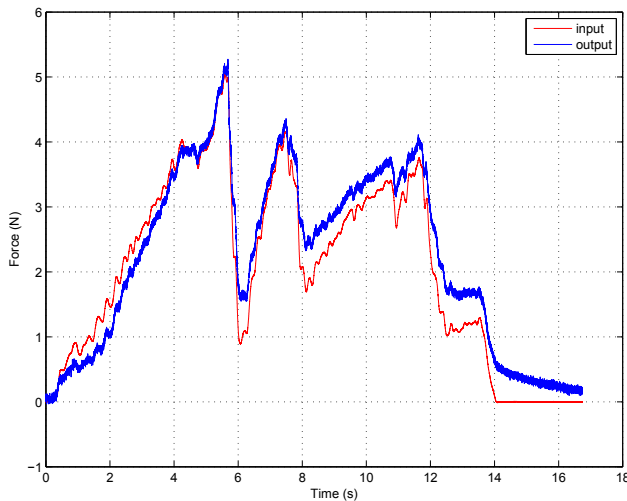


Fig. 13. Response to the experimental force profile as input.

applied force and the force measured from the prototype sensor is actually quite satisfactory. It was obtained with the gain identified from the harmonic response at 0.5Hz. The use of the gain obtained in static conditions, which is affected by a very slow drift would provide less satisfactory results. In the figure, most of the haptic cues are present: the transients which are very important to feel ruptures of tissues appear clearly, with very limited attenuation. The small variations in magnitude are hardly perceptible and will not affect the haptic feedback if such a sensor is used to provide force feedback in a bilateral teleoperation scheme. Given the nature of the measured signals, the best model of the sensor on a given frequency range could be characterized. It should also be noted that it remains nevertheless a delicate task because the spectral analysis of a typical signal does not necessarily fully inform on the perceived haptic features.

V. CONCLUSION

A novel force sensor compatible with the CT-scanner was developed using a compliant version of the Sarrus mechanism and strain gages as the force sensing principle. The design of the force sensor ensured that many stringent constraints such as through hole for the passage of the needle, radiolucency, compactness, high stiffness were satisfied. The numerical model of the force sensor verified its theoretical working in the elastic range. It also helped choose the structural design parameters for the fabrication of a initial prototype for the preliminary experiments and characterization. The static and dynamic responses of the force sensor were evaluated. The force sensor after calibration gave a quite satisfactory fit between output and a realistic force profile as input. The important events such as tissue rupture marking sharp decline in the force levels were satisfactorily reproduced. Hence, this force sensor could be used for haptic feedback during needle insertion procedures.

Though the simple elastic model of the force sensor provided an initial model for describing the results, it cannot model the hysteresis and describe the non-linearities in

the results. This behavior would be best described by a viscoelastic model, the modeling of which would form an important part of the future work. Also, the test bench will be expanded to cover the effect of moment load disturbance along the needle axis.

ACKNOWLEDGMENT

The authors acknowledge the support of the Image-guided Hybrid Surgery Institute (IHU Strasbourg) and the Foundation ARC. This work has been sponsored by the French government research program Investissements d'Avenir through the Robotex Equipment of Excellence and Labex CAMI (ANR-10-EQPX-44 and ANR-11-LABX-0004).

REFERENCES

- [1] O. Piccin, L. Barbé, B. Bayle, M. de Mathelin, and A. Gangi, "A force feedback teleoperated needle insertion device for percutaneous procedures," *The International Journal of Robotics Research*, vol. 28, no. 9, pp. 1154–1168, Sept. 2009. [Online]. Available: <http://ijr.sagepub.com/content/28/9/1154>
- [2] R. Gassert, R. Moser, E. Burdet, and H. Bleuler, "MRI/TMRI-compatible robotic system with force feedback for interaction with human motion," *IEEE/ASME Transactions on Mechatronics*, vol. 11, no. 2, pp. 216–224, Apr. 2006.
- [3] P. Polygerinos, L. Seneviratne, R. Razavi, T. Schaeffter, and K. Althoefer, "Triaxial catheter-tip force sensor for MRI-Guided cardiac procedures," *IEEE/ASME Transactions on Mechatronics*, vol. 18, no. 1, pp. 386–396, Feb. 2013.
- [4] O. Piccin, N. Kumar, L. Meylheuc, L. Barbé, and B. Bayle, "Design, development and preliminary assessment of grasping devices for robotized medical applications," pp. 65–73, Aug. 2012. [Online]. Available: <http://dx.doi.org/10.1115/DETC2012-70634>
- [5] B. Maurin, L. Barbé, B. Bayle, P. Zanne, J. Gangloff, M. Mathelin, A. Gangi, L. Soler, and A. Forgiione, "In vivo study of forces during needle insertions," in *Perspective in Image-guided Surgery: Proceedings of the Scientific Workshop on Medical Robotics, Navigation, and Visualization (MRNV 2004)*, 2004, p. 415–422.
- [6] A. Graña, A. Sánchez, N. Zemiti, and P. Poignet, "Modelling and control of an ERF-Based needle insertion training platform," in *Information Processing in Computer-Assisted Interventions*, ser. Lecture Notes in Computer Science, D. Stoyanov, D. L. Collins, I. Sakuma, P. Abolmaesumi, and P. Jannin, Eds. Springer International Publishing, Jan. 2014, no. 8498, pp. 31–40.
- [7] H. Su and G. Fischer, "A 3-axis optical force/torque sensor for prostate needle placement in magnetic resonance imaging environments," in *IEEE International Conference on Technologies for Practical Robot Applications, 2009. TePRA 2009*, 2009, pp. 5–9.
- [8] R. Gassert, D. Chapuis, H. Bleuler, and E. Burdet, "Sensors for applications in magnetic resonance environments," *IEEE/ASME Transactions on Mechatronics*, vol. 13, no. 3, pp. 335–344, 2008.
- [9] M. Yip, S. Yuen, and R. Howe, "A robust uniaxial force sensor for minimally invasive surgery," *Biomedical Engineering, IEEE Transactions on*, vol. 57, no. 5, pp. 1008–1011, May 2010.
- [10] S. Shah, A. Kapoor, J. Ding, P. Guion, D. Petrisor, J. Karanian, W. F. Pritchard, D. Stoianovici, B. J. Wood, and K. Cleary, "Robotically assisted needle driver: evaluation of safety release, force profiles, and needle spin in a swine abdominal model," *International Journal of Computer Assisted Radiology and Surgery*, vol. 3, no. 1-2, pp. 173–179, June 2008. [Online]. Available: <http://link.springer.com/article/10.1007/s11548-008-0164-2>
- [11] D. M. Stefanescu, *Handbook of Force Transducers: Principles and Components*. Springer, May 2011.
- [12] A. Hoover and R. Fearing, "Analysis of off-axis performance of compliant mechanisms with applications to mobile millirobot design," in *Intelligent Robots and Systems, 2009. IROS 2009. IEEE/RSJ International Conference on*, Oct 2009, pp. 2770–2776.